Cable surface preparation; chemical, physical and electrical characterization and impact on breakdown voltage

Espen **DOEDENS**, Markus **JARVID**, Nexans Norway AS, Norway,
espen.doedens@nexans.com, markus.jarvid@nexans.com

Stanislaw **GUBANSKI**, Chalmers University of Technology, Sweden,
stanislaw.gubanski@chalmers.se

Christian **FROHNE**, Nexans Germany GmbH, Germany,
christian.frohne@nexans.com

ABSTRACT

Material interfaces play a crucial role in the performance of HVDC cable systems. This contribution analyzes the impact of different preparation methods on the XLPE surface characteristics and the surfaces' behaviour under DC stress. Three different surface types were characterized with regards to roughness, topography, surface free energy, breakdown strength and charge decay characteristics. Both the surface free energy and the roughness seem to have an impact on the electrical properties of the surface. Charge decay measurements on the surfaces show conduction properties with the same field dependencies controlled by field enhanced mechanisms.

KEYWORDS

HVDC extruded, cable accessories, cable surface, cable preparation, physical interface, cable peelings, roughness, surface free energy, surface topography, DC breakdown voltage, surface charge decay.

INTRODUCTION

The recent expansion in the utilization of renewable energy sources poses new challenges to the European power grid. In order to overcome challenges such as remoteness of these energy sources, and the fluctuations of the power output, many HVDC transmission systems are implemented into the grid. These transmission systems can use mass impregnated (MI) cables, cross-linked polyethylene (XLPE) cables or overhead lines. The extruded XLPE HVDC cables have recently entered the market [1], and benefit from having factory tested pre-molded joints and terminations. This feature, amongst others, makes it a desired product on the market.

Some accessories featured in the HVDC extruded cable system are land joints, field joints, repair joints and terminations. What all these accessories have in common is that they have a physical interface [2], consisting of the mating between a pre-molded accessory body and the exposed cable insulation surface. The cable insulation surface is exposed through a procedure, in which the outer semiconductive layer is removed and the insulation surface is treated to become smooth enough to prevent any partial discharge phenomena in the mated interface. This study aims to characterize such surfaces, as recent research has shown a link between cable surface preparation method and DC breakdown voltage exists [3]. The preparation methods investigated in this research are: abrasion, cutting and remolding and these are chosen for their reproducibility and direct applicability for full-scale cable accessories. Cable peelings were used in order to replicate the surface characteristics of the full-scale accessories. The geometry and preparation of a cable peeling is shown in Fig. 1.

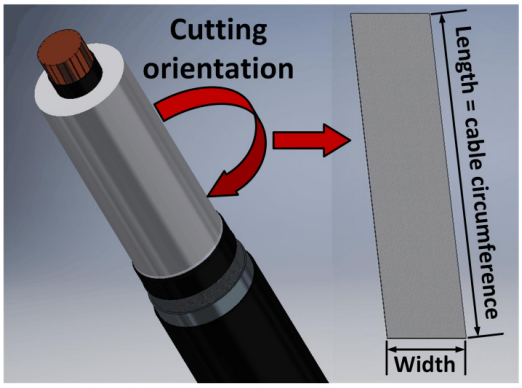

Fig. 1: Cable peelings cut from the surface of HVDC extruded cable ends

THEORY

Depending on the preparation method, different cable surface characteristics can be created, such as roughness, surface states, surface layer morphology and chemical concentration gradients.

Surface free energy

The surface free energy (SFE) is quantified by the disrupted bonds created through the surface preparation process. As the disrupted bonds will interact with any liquids and solids contacting the surface, the SFE can be determined by means of sessile drop technique, in which a droplet of known surface tension is placed on the surface and the contact angle is measured. The SFE is sensitive for both roughness and surface states making it an interesting assessment method for polymeric surfaces. From a measured contact angle, the SFE can be calculated by using Neumann equation:

$$\sqrt{(\gamma_s/\gamma_l)}(1-\beta_2(\gamma_l-\gamma_s)^2) = 0.5(1+\cos\theta_a) \quad (1)$$

where θ_a is the advancing contact angle, γ_s is the SFE, γ_l is the liquids surface tension and β_2 is a predetermined parameter. Determination of SFE is also possible through measurement of contact angle hysteresis [4]:

$$\gamma_s = \gamma_l(\cos\theta_r - \cos\theta_a)\frac{(1+\cos\theta_a)^2}{(1+\cos\theta_r)^2-(1+\cos\theta_a)^2} \quad (2)$$

where θ_r is the receding contact angle. Increased surface roughness is also known to improve the wettability, according to the Wenzel state, until the roughness is so high that air is present underneath the droplet, at which the wettability is reduced, according to the Cassie-Baxter state:

$$\cos\theta_m = rf\cos\theta_Y + (f-1) \quad (3)$$

where θ_m is the measured advancing contact angle, θ_Y is Young's (advancing) contact angle of an infinitely smooth surface, r is the roughness ratio and f is the fraction of the droplet in contact with the surface.

Surface charge and injection phenomena

In charge decay measurements surface charge can be measured over time using a capacitive probe. The charge can be deposited on the surface through corona charging or other methods. For estimating the conductivity from a charge decay measurement, equation (4) can be used, which is a combination of ohms law and the continuity equation for electric currents.

$$\frac{\partial V}{V\partial t} = -\frac{\sigma}{\varepsilon} \quad (4)$$

Here V is the measured surface potential, σ is the conductivity and ε is the permittivity of the sample. When analyzing the field dependency of the conductivity in such a measurement, it is useful to plot $log(J)$ against $\sqrt{E}$ as Schottky injection shows such a dependency:

$$J = (1-R)A^*T^2 e^{\frac{e}{kT}(\chi-\phi_m+\sqrt{\frac{eE}{4\pi\varepsilon_o\varepsilon_r}})} \quad (5)$$

where R is the reflection probability, A^* is the Richardson's constant, T is the temperature, ϕ_m is the metal work function and χ is the electron affinity of the insulator. The field dependency is originating from the barrier lowering effect [5] and is shared with the Poole-Frenkel effect for bulk conduction, thus these two phenomena cannot be fully separated. Surface roughness may be taken into account by introducing a Field enhancement factor (FEF) into equation (5) as is done by Taleb et al. [6], as long as this does not cause the maximum barrier position to approach interatomic distances.

EXPERIMENTAL

All samples except the breakdown test samples where cable peelings, in which a full-scale DC grade XLPE cable end was prepared and the peelings were cut utilizing a rotational cutting tool with a specially designed blade, as shown in Fig. 1. For the breakdown test samples, the same preparation methods were used, but applied to a MV-sized cable end. The abraded, cut and remolded surfaces were created with the preparation method, while backside surfaces originate from cutting in the peeling process. The backside is thus different from the other surfaces in that it cannot be found and replicated in real accessories, and that each cable peeling has such a surface on one of the sides.

After manufacturing, the cable peelings were stored in an incubator at around 10-12 % RH in order to eliminate the influence of moisture on the measured properties.

Optical profilometry was applied, using white light interferometry by means of Wyko RST plus interferometer. Three minutes of gold sputtering was required in order to ensure the necessary reflective capabilities for the measurement. The surface profile of each surface was then filtered in order to remove the major surface texture not influencing the contacting properties of the surface. A total of 5 measurements were performed for each surface type.

Contact angle measurements were performed using sessile drop measurements in which both advancing and receding contact angles were determined along and across the surface texture. From the contact angle measurements the surface free energies (SFE) were calculated. The calculated SFEs were compared with a DYNE test set, in which the liquid surface tension required for full wetting ($\theta_m=0$) is found. The highest surface tension that still wets the surface for more than 2 seconds, should correspond to the SFE of the sample (without the impact of surface roughness).

For scanning electron microscope observations (SEM), 1 min gold sputtering was applied to the sample surface. The SEM was performed using secondary electrons (SE).

For the ramped DC breakdown tests, the same sample geometry was used as in [3], and the exposed cable ends were connected to a DC generator. No accessories or components were placed onto the cable surface, creating a surface towards ambient air. The test cell was dehumidified in order to reduce the risk of flashovers during the tests. After the tests, microscopic observations were used to investigate the breakdown characteristics and to determine the sample thickness at the breakdown position. The latter was used to calculate the average electric field during the test.

Charge decay measurements were performed in a dedicated test cell [7]. The test cell was adapted to fit the geometry of the cable peelings and dehumidified, using CaCl solution, which resulted in a relative humidity below 18% during the tests. The dehumidification was used in order to reduce the possibility of having any adsorbed polar layers (such as water), which would influence the charge decay measurement [8]. The backsides of the cable peelings were gold sputtered for 6 min to ensure good electrical contact between the sample and the ground plane. The samples were charged with -5 kV and -10 kV negative corona voltages from a needle tip for 2 minutes, and were then moved to make a line scan for each measurement. The resting position of the capacitive probe was away from the measurement area. By obtaining many line scans over time, the development of the charge distribution could be measured against time, allowing for distinguishing between bulk and surface conduction processes.

RESULTS

The cable peelings have been characterized, and most of their properties are expected to mimic the properties of HVDC cable accessory interfaces. The peroxide decomposition product content and any other characteristics that are influenced by sample thickness are examples of where the properties may differ.

HPLC measurements

Before peeling a byproduct content of 585±4 ppm cumyl alcohol and 198.5±2.5 ppm acetophenone was measured in the surface area of the prepared cable sample. After 3 months of storing the cable peelings in the incubator the byproduct content had reduced to 180±17 ppm cumyl alcohol and 43.5±4.5 ppm acetophenone for a thicker cable peeling (0.7 mm thickness) and 138.5±3.5 ppm cumyl alcohol 26±1 ppm acetophenone for a 0.4 mm thick cable peeling. No α-metyl styrene, dicumyl peroxide or methane was detected. The low level of byproduct content in these samples is caused by the fact that the cable was priory degassed according to normal industrial methods.

Optical profilometry

The three dimensional surface parameters of the polymeric surfaces are displayed in Fig. 2. What the results show is that there exists a significant difference in the roughness of these surfaces, where abraded is the roughest and remolded is approaching roughness levels found in semiconductor devices. This is relevant as Schottky and Fowler-Nordheim injection laws are derived for such low roughness levels (or infinitely low roughness levels). The rougher surfaces might deviate through the introduction of localized electric field enhancements.

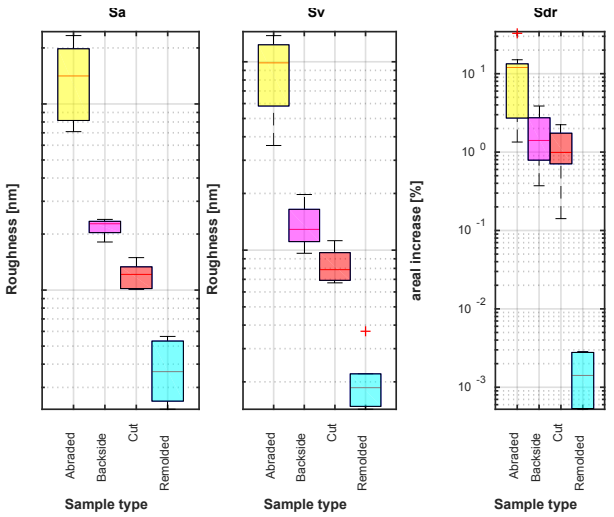

Fig. 2: Arithmetic mean height (Sa, left), maximum pit height (Av, middle) and developed interfacial area ratio (Sdr, right) of the surfaces. The y axis features a logarithmic scale

The developed interfacial area ratio was further used for SFE calculation through the Cassie-Baxter equation.

Surface free energy measurement

The observed contact angles using deionised water are shown in Fig. 3, along and across the surface texture. The fairly low standard deviation found in the measurements shows good homogeneity over the sample surface. Heterogeneity is found depending on the observation direction, which corresponds to the influence of the surface texture on the measurement.

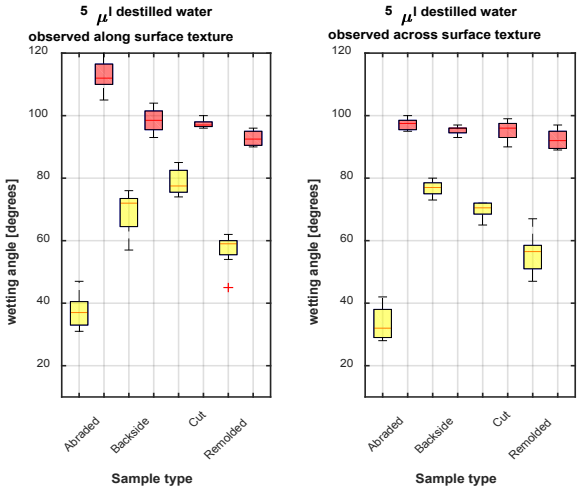

Fig. 3: Measured Advancing and receding contact angles for the different surfaces for 5µl deionised water droplets observed along surface texture (left) and observed across surface texture (right)

As illustrated in Fig. 4, three methods described in the theory section were used for calculations of SFE. It shows that the use of Neumann method (1) and contact angle hysteresis (2) provides comparable results. However, these methods fail to include the effect of surface roughness and air present underneath the droplet according to the Cassie-Baxter state. For this reasons the Young's contact angles were calculated by equation (3), and inserted into the Nuemann method. The roughness parameters were estimated though optical profilometry, while optical microscopy was used to determine the contact area fraction. A large data spread is observed for the abraded samples, which were the only surfaces where air underneath the droplet was observed.

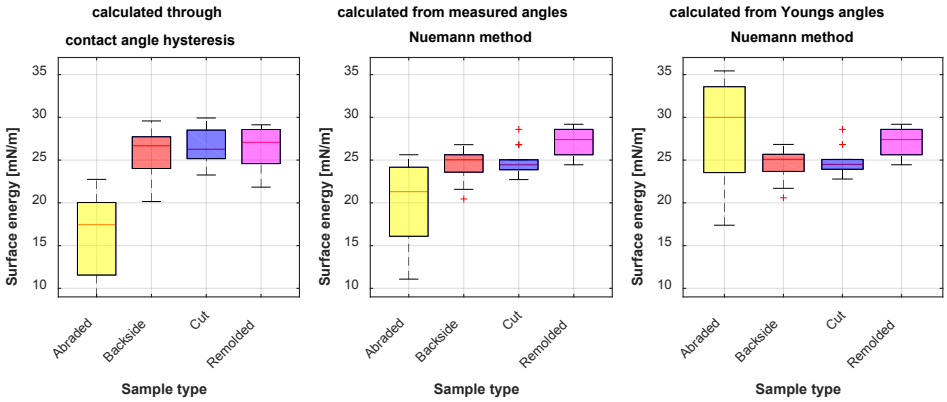

Fig. 4: Calculated SFE from contact angles using methods: contact angle hysteresis (left), Nuemann method (centre) and Cassie baxter equation together with Neumann method (right)

For the DYNE test, no air can be present under the liquid as the liquid wets, so only the roughness ratio of the surface was used for SFE determination, resulting in 32.5, 28.5, 26.7 and 27 mN/mm of SFE respectively for abraded, backside, cut and remolded. These results somewhat match the SFE calculated from the Neumann method using the Cassie-Baxter equation displayed in Fig. 4 (right hand side).

SEM

SEM observations were used in order to further investigate the surface texture and topography. The results are shown in Fig. 5.

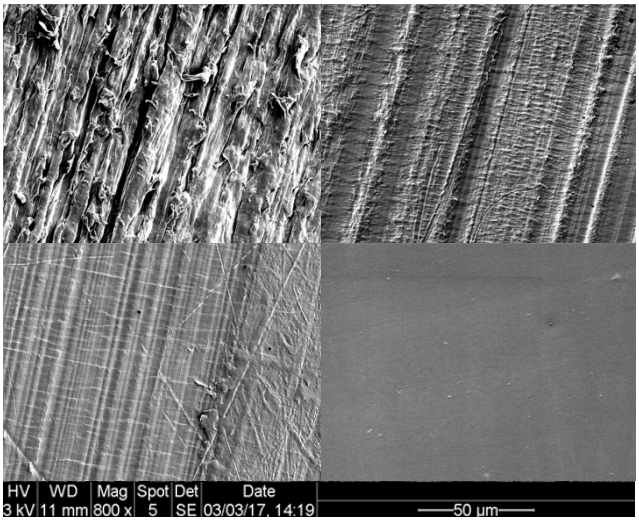

Fig. 5: SEM of surface samples utilizing secondary electrons (SE) at 800x magnification. Abraded (top left), backside (top right), cut (bottom left) and remolded (bottom right)

The abraded surface texture shows scratches in the abrasion direction as well as small folded peaks, also observed by [9]. It is likely that these beaks originate from some kind of yielding process, as polymeric particles are pulled off from the surface. The backside and cut samples in Fig. 5 show striations in the cutting direction, originating from the shape of the cutting knife edge. Lines parallel to the cutting edge are also observed which could be caused by fracture mode of material removal during the cutting operation. These lines do not resemble any severe knife chatter traces; as such traces would be indicated by fully parallel lines and introduce a higher degree of roughness to the texture. The remolded surface is smooth and the texture is likely a replication of the polymeric contact film used in this preparation method.

DC breakdown tests

The results of the DC breakdown tests on cable ends are presented in a Weibull plot in Fig. 6.

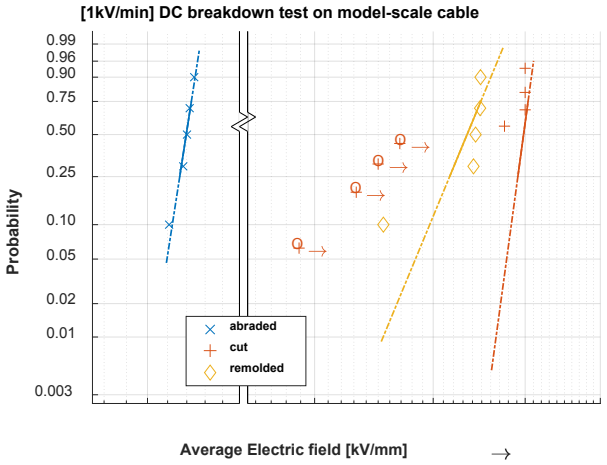

Fig. 6: Ramped DC breakdown tests on cable ends. Negative Polarity was used, circles and arrows indicate flashovers which were censored. Notice also the break in the x-axis

It is shown that the different surface preparation methods resulted in very different DC performance, whereas the abraded surface broke down at a field level somewhere above the onset of space charge injection into DC cables [10]. The remolded and cut surfaces broke down at a significantly higher field level, which also resulted in different breakdown channel appearances as shown in Fig. 7. For abraded surfaces, the average electric field was low, and this resulted in a DC breakdown channel propagating from the outer surface towards the inner semiconductive layer of the cable. For the remolded and cut surfaces, besides the main breakdown channel, also tangential and axial progagating channels were found in a layer 0.2-0.5 mm below the surface of the cable.

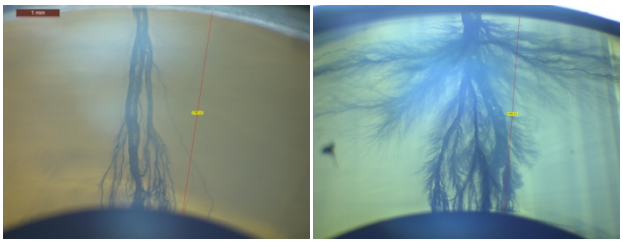

Fig. 7: Breakdown channel of cables with abraded (left) and cut (right) surfaces

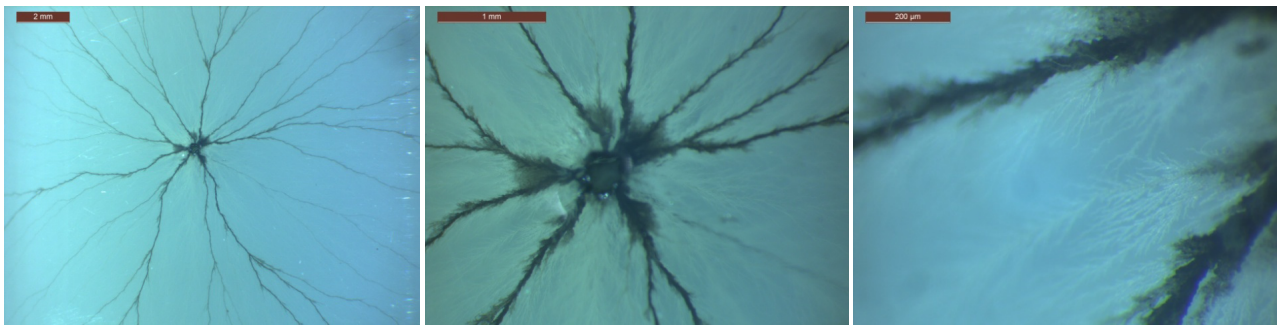

Fig. 8: breakdown channel for a remolded cable end seen from above, at low magnification (left), medium magnification (middle) and high magnification (right). Notice also white traces present in the breakdown

As shown in Fig. 8, the breakdown channels below the surface propagate somewhat symmetrically in all directions. The bigger channels have black carbonized deposits, but also smaller whitish discharge traces can be detected in between these branches that remain invisible in the observation in Fig. 7 due to the refraction of the light when looking through a thicker specimen.

Surface charge decay measurements

For the surface charge decay measurement, it is most interesting to investigate the averaged electric field in the samples, as the peeling method fails to create samples of identical and uniform thickness. The electric field decay is found by dividing over sample thickness along the line scan, and is shown for an abraded sample (sample G) in Fig. 9 below.

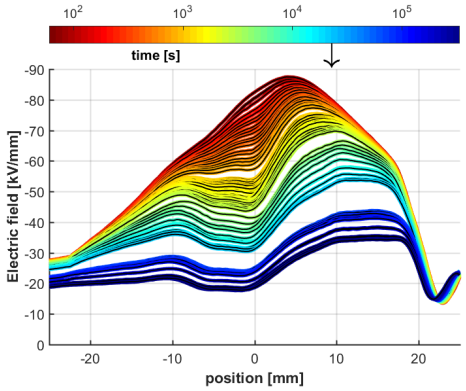

Fig. 9: Charge decay profile of sample G, an abraded sample charged with -10kV corona

The maximum electric is not found at the corona charging position, indicated with an arrow in Fig. 9, due to non-uniform thickness in this sample. The fastest decay *(∂E/∂t)* is also found away from the charging position, and no significant surface conduction can be seen. This indicates that the measured charge decay is due to conduction through the sample. The averaged electric field for all samples decay is displayed versus time in Fig. 10.

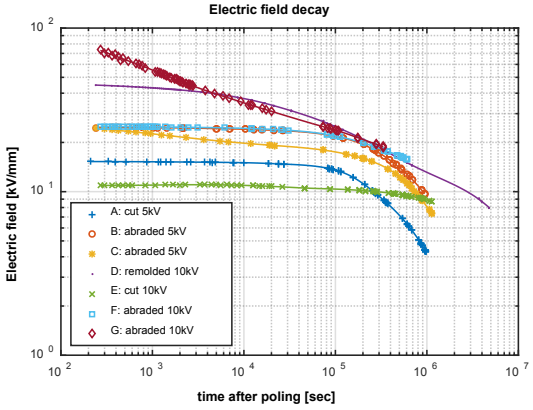

Fig. 10: Average electric field (voltage/sample thickness) decay during measurements

The decay in the DC grade XLPE is extremely slow, which is in line with conductivity measurements on this material. From the decay measurements the conductivity was estimated using equation (4), and used for making a Schottky plot as shown in Fig. 11. Note that the decay occurs from left to right in Fig. 10 but from right to left in Fig. 11. Some initial polarization of the material, or charge injection from the ground electrode, is noticed in each measurement for the first few hours ($t<10^4$ *sec*), resulting in an increased current by around one decade. After this initial decay process most measurements follow the same trends. Sample C deviates from this pattern by having its initial current around three decades higher. The thickness of sample E was purposely chosen to be as thick as possible in order to once again assess magnitude of ambient charge recombination during the tests. As sample E decayed along the same line as for sample D and F in Fig. 11, the impact of ambient recombination is believed to be minimal, as ambient recombination depends on the external field and not the electric field inside the sample.

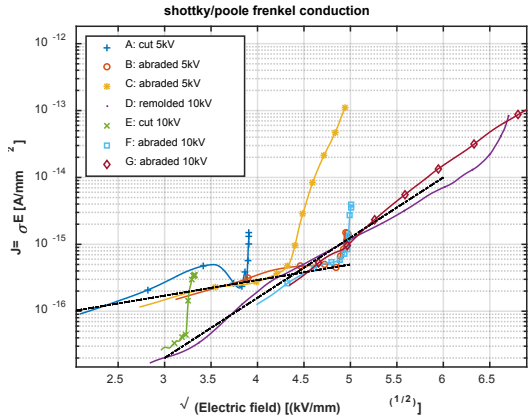

Fig. 11: Schottky plot for the decay characteristics

There is a difference in decay rate in the Schottky plot between -5 kV and -10 kV poled samples, visualized with dash-dotted lines. This difference can originate from different charging conditions where the negatively charged ions can either remain on the surface, transfer to the surface layer or transfer to the bulk of the material [11]. A different position of the initial charge can thus affect the contribution of Schottky injection and Poole-Frenkel effect to the total conduction process, as both the phenomena have similar field dependency.

DISCUSSION

The electrical breakdown strength seems to depend on the roughness parameters, as the rough samples inhibit very low breakdown strength. However, the maximum pit height determined through optical profilometry shows that the maximum void size for any of these surfaces should be too small for initiating any partial discharge activities. Calculated breakdown strength in such cavities (using Paschen's law), should exceed the breakdown strength observed in this study. The breakdown strength could instead be related to charge injection processes, affecting the charge distribution in the insulation system.

For samples below a certain surface roughness threshold, the breakdown dependency on roughness seems to vanish. It could be the case that below this threshold, the breakdown strength is no longer related to surface roughness and instead dependent on surface states and/or intrinsic material properties. Verification against the exact surface topography is still needed as the measured surface parameters are insensitive in differentiating amongst certain surface features.

The calculated SFE shows some differences amongst the

smoother surfaces, where the remolded surface seems to have a slightly higher SFE than the cut surfaces. As SFE is affected by the amount of surface states, this could mean that there is a different amount of surface states for the remolded and cut surfaces. Whether this explains the lower breakdown strength of the remolded surface, still remains to be confirmed with tests on additional sample types.

Some interesting breakdown phenomena have been shown, but how these relate to the surface properties is not yet known. As the traces were found in a layer at a fixed distance from the surface, they could originate from a phenomena occurring in this layer. An excess space charge accumulation could be present there. In such a case the main breakdown channel could act as the grounding point, creating a high electric field towards the accumulated charge. The accumulated charge then discharges itself towards the main breakdown channel. The breakdown appearance could thus be related to a charge accumulation in the material, though this remains to be verified with additional studies.

One of the abraded samples (sample C) deviated from the other samples in the charge decay measurement. The origin of this deviation and whether it can be related to other electrical properties of the surface is left to be investigated with additional sample tests.

The degassing of by-products during sample storage is a commonly known problem for plate/peeling samples and is known to influence electrical properties. For the samples in this study the content prior to peeling and storing the samples was already inherently low. Such an influence is therefore not believed to be the main contributor towards the big differences in surface properties reported here.

CONCLUSION

The cable surfaces have been characterized with regards to roughness, topography, SFE and breakdown voltages. Rough surfaces seem to have a lower breakdown voltage, but for smoother surfaces this dependency seems to disappear. This indicates that roughness and surface states might affect the electrical properties through different processes. Charge decay measurements show conduction properties controlled by field enhanced mechanisms, as Schottky injection or the Poole-Frenkel effect.

FUTURE WORK

Improvements to the cable peeling method are to be made in order to create thinner and wider samples of more uniform thickness. Such improved samples should allow for DC breakdown and conductivity measurements on the peelings, adding to the surface characterization, and determining the origin of the spread of breakdown voltages observed on the MV cable ends.

Further utilization of the 3D roughness measurements is planned by using the data to obtain FEF:s for investigating the impact on Schottky and Fowler-Nordheim injection phenomena, as is investigated in [6].

The full I-V characteristics of these surfaces and also other theoretically interesting surfaces remain to be statistically validated over a wide range of electric fields.

Acknowledgments

Nexans Norway AS is acknowledged for the financial support of these research activities. Also the personnel from the Nexans Halden R&D lab is acknowledged for carrying out the DC breakdown tests on MV cables and their aid in the surface preparation and peeling manufacturing.

REFERENCES

[1] “Nexans supplies 320 kV cables for ‘DolWin6’ offshore DC link to TenneT - Nexans.” [Online]. Available:http://www.nexans.com/eservice/Corporate-en/navigatepub_0_-35910_297_40_11229/TenneT_awards_Nexans_a_100_million_worth_contract_.html. [Accessed: 01-Aug-2017].

[2] P. Morshuis, “Interfaces: To be avoided or to be treasured? What do we think we know?,” in *2013 IEEE International Conference on Solid Dielectrics (ICSD)*, 2013, pp. 1–9.

[3] E. H. Doedens, N. B. Frisk, M. Jarvid, L. Boyer, and S. Josefsson, “Surface preparations on MV-sized cable ends for ramped DC breakdown studies,” in *2016 IEEE Conference on Electrical Insulation and Dielectric Phenomena (CEIDP)*, 2016, pp. 360–362.

[4] E. Chibowski, “Surface free energy of a solid from contact angle hysteresis,” *Adv. Colloid Interface Sci.*, vol. 103, no. 2, pp. 149–172, Apr. 2003.

[5] Len A. Dissado and J. C. (John C. . Fothergill, *Electrical degradation and breakdown in polymers*. P. Peregrinus, 1992.

[6] M. Taleb, G. Teyssedre, and S. Le Roy, “Role of the interface on charge build-up in a low-density polyethylene: Surface roughness and nature of the electrode,” in *2009 IEEE Conference on Electrical Insulation and Dielectric Phenomena*, 2009, pp. 112–115.

[7] S. Alam, Y. Serdyuk, and S. Gubanski, “Potential decay on silicone rubber surfaces affected by bulk and surface conductivities,” *IEEE Trans. Dielectr. Electr. Insul.*, vol. 22, no. 2, pp. 970–978, Apr. 2015.

[8] T. J. Lewis, “Electrical Effects at Interfaces and Surfaces,” *IEEE Trans. Electr. Insul.*, vol. EI-21, no. 3, pp. 289–295, Jun. 1986.

[9] M. Hasheminezhad and E. Ildstad, “Application of contact analysis on evaluation of breakdown strength and PD inception field strength of solid-solid interfaces,” *IEEE Trans. Dielectr. Electr. Insul.*, vol. 19, no. 1, pp. 1–7, Feb. 2012.

[10] D. Fabiani *et al.*, “Polymeric HVDC Cable Design and Space Charge Accumulation. Part 1: Insulation/Semicon Interface,” *IEEE Electr. Insul. Mag.*, vol. 23, no. 6, pp. 11–19, Nov. 2007.

[11] T. J. Lewis, “Electrical Effects at Interfaces and Surfaces,” *IEEE Trans. Electr. Insul.*, vol. EI-21, no. 3, pp. 289–295, Jun. 1986.

GLOSSARY

HVDC: High Voltage Direct Current
XLPE: Crosslinked polyethylene
MI: Mass impregnated
SEM: Scanning Electron Microscopy
MV: Medium Voltage
FEF: Field enhancement factor